Materials Advances

ROYAL SOCIETY OF CHEMISTRY

COMMUNICATION

View Article Online
View Journal | View Issue

Cite this: *Mater. Adv.*, 2022, 3, 4542

Received 13th April 2022,
Accepted 3rd May 2022

DOI: 10.1039/d2ma00418f

rsc.li/materials-advances

A rapid construction strategy of $NaYF_4$:Yb,Er@CDs nanocomposites for dual-mode anti-counterfeiting†

Haopeng Wei,‡[ab] Yihao Zheng,‡*[ab] Xingcai Zhang,[cd] Ping Liang,[ab] Xiaokai Xu,[ab] Chaofan Hu,[ab] Xuejie Zhang,[ab] Bingfu Lei,[ab] Yingliang Liu*[ab] and Jianle Zhuang*[ab]

A rapid construction strategy is for the first time developed to achieve the composite structure of $NaYF_4$:Yb,Er and carbon dots (CDs) through electrostatic interactions in only half a minute. The resulting $NaYF_4$:Yb,Er@CDs nanocomposites have superior dual-mode luminescence properties, showing promising application prospects in the field of advanced optical anti-counterfeiting.

Introduction

Optical anti-counterfeiting is a common and mature anti-counterfeiting method, which is widely used in many fields in our daily life such as banknotes, documents, invoices, medicine, tobacco, alcohol, electronic products, and so on.[1–4] However, currently, counterfeit and shoddy products are increasing day by day, and traditional optical anti-counterfeiting technology is facing a huge challenge.[5,6] As we all know, traditional optical anti-counterfeiting mainly uses single-mode fluorescent materials under ultraviolet (UV) excitation, which is very easy to be imitated and faked by some counterfeiters.[7] Therefore, in order to meet the urgent demand for advanced anti-counterfeiting technology in many fields, it is of great significance to develop new optical anti-counterfeiting materials with multimode luminescence properties.[8,9]

To the best of our knowledge, the currently reported luminescent materials for optical anti-counterfeiting have some problems. For traditional semiconductor quantum dots, the prominent toxicity problem restricts their development in the application of anti-counterfeiting.[10,11] Perovskite nanocrystals exhibit lots of limitations in the anti-counterfeiting field due to their poor environmental stability, harsh synthesis process, and high cost.[12,13] There are also many unfavorable factors for the application of organic luminescent materials in anti-counterfeiting, such as complicated molecular design, poor air stability, and non-negligible toxicity.[14,15] Recently, carbon dots (CDs) have attracted intense attention and interest in security applications such as anti-counterfeiting, information encryption, and fingerprint identification, because of their excellent optical properties, easy preparation and structural regulation, good photostability, environmental friendliness, and low toxicity and cost.[16–20] Nevertheless, the single down-conversion (DC) luminescence mode and the well-known aggregation-caused quenching (ACQ) effect still make it difficult for pure CDs to directly achieve more complex anti-counterfeiting.[21–23] To this end, we conceive combining CDs with upconversion (UC) materials to achieve dual-mode optical anti-counterfeiting, which can improve the safety factor and increase the difficulty of being forged. It is well known that lanthanide-doped upconversion nanoparticles (UCNPs) have excellent upconversion luminescence (UCL) properties and easily modified surface structures.[24–27] However, it is difficult to combine UCNPs and CDs by constructing a single core–shell structure because of their lattice mismatch. In order to overcome this problem, many research groups have tried other methods. Wu *et al.* and Song *et al.* incorporated as-prepared UCNPs into the reaction system of CDs, in which the CDs were synthesized *in situ* and attached to the surface of the UCNPs.[28,29] Unfortunately, this kind of construction is unstable, and the CDs could fall off relatively easily. Our group and others have tried to embed the CDs into the silica shell on the surface of UCNPs to obtain stable dual-mode luminescent

[a] *Key Laboratory for Biobased Materials and Energy of Ministry of Education/ Guangdong Provincial Engineering Technology Research Center for Optical Agriculture, College of Materials and Energy, South China Agricultural University, Guangzhou 510642, China. E-mail: chemzhengyh@163.com, tliuyl@scau.edu.cn, zhuangjl@scau.edu.cn*

[b] *Guangdong Laboratory for Lingnan Modern Agriculture, Guangzhou 510642, China*

[c] *School of Engineering and Applied Sciences, Harvard University, Cambridge, MA, 02138, USA*

[d] *School of Engineering, Massachusetts Institute of Technology, Cambridge, MA, 02139, USA*

† Electronic supplementary information (ESI) available. See DOI: https://doi.org/10.1039/d2ma00418f

‡ These authors contributed equally to this work.

nanocomposites, but a complex sol–gel method was required in the preparation process.[30,31] Xing *et al.* achieved the covalent coupling of carboxyl groups on the surface of CDs and amine groups on the surface of UCNPs through the amidation reaction.[32] This method is limited due to its long reaction time, low efficiency, high technical requirements and poor reproducibility. More importantly, the surface functional groups involved in the reaction can change the surface state of CDs, which will affect or even quench the luminescence of CDs. Therefore, it is highly desirable to construct a stable dual-mode luminescent nanocomposite by a facile and efficient method that does not change the surface groups of CDs.

In this work, we propose a novel and rapid strategy to construct composite structures of $NaYF_4$:Yb,Er UCNPs and CDs through electrostatic interactions. The surface potentials of the as-prepared carboxylate radical-functionalized CDs and branched PEI-modified UCNPs are opposite, which provides an electrostatic driving force for rapid adsorption. After the addition of $NaYF_4$:Yb,Er UCNPs to the CD solution, the CDs immediately begin to be adsorbed by $NaYF_4$:Yb,Er, and the entire adsorption process can be completed in only half a minute. The branched PEI ligand chains on the surface of $NaYF_4$:Yb,Er not only strongly adsorb CDs to form a stable composite structure, but also act as a matrix to disperse CDs and inhibit their aggregation. The resulting $NaYF_4$:Yb,Er@CDs nanocomposites show excellent dual-mode luminescence properties and great application potential in the field of anti-counterfeiting.

Results and discussion

The CDs were synthesized by a solvothermal method using citric acid as the carbon source and thiourea as the nitrogen source. The surface of the as-prepared CDs contains abundant negative ionized carboxylate radicals. The $NaYF_4$:Yb,Er UCNPs were synthesized by a solvothermal method with branched PEI as the surface ligand. Since there are lots of amine groups on the PEI polymer chains, the surface of $NaYF_4$:Yb,Er is positively charged. After $NaYF_4$:Yb,Er UCNPs were added to the CD solution, it could be observed that the luminescence of the CD solution decayed drastically under UV light as the CDs were rapidly adsorbed by $NaYF_4$:Yb,Er. Importantly, the process was completed thoroughly only by manual shaking for half a minute. After standing, removing the supernatant, and freeze-drying, $NaYF_4$:Yb,Er@CDs nanocomposites with dual-mode (UC and DC) luminescence properties were obtained (Scheme 1 and Fig. S1, ESI†).

The morphology and structure were characterized by transmission electron microscopy (TEM), high-resolution transmission electron microscopy (HRTEM), and energy dispersive spectroscopy (EDS) elemental mapping. As shown in Fig. 1a, the as-prepared CDs are uniform and monodisperse spherical particles with a diameter of about 2.1 nm (Fig. S2, ESI†). The HRTEM image of CDs in the inset of Fig. 1a exhibits clear lattice fringes with a 0.21 nm spacing, which is close to the (100) plane of graphite carbon.[33–35] It can be observed from Fig. 1b that the as-prepared $NaYF_4$:Yb,Er UCNPs show a typical sphere-like structure of about 50 nm size. The HRTEM images corresponding to the red squares in Fig. 1c demonstrate apparent lattice fringes with 0.31 nm and 0.25 nm spacing, which can be assigned to the (111) plane of cubic $NaYF_4$ and the (020) plane of graphite carbon for the adsorbed CDs, respectively.[33–35] The high-angle annular dark field (HAADF)-STEM image (Fig. 1d) and EDS elemental mapping (Fig. 1e–k) of $NaYF_4$:Yb,Er@CDs composites further confirm the preferential distribution of the CDs containing oxygen and sulfur elements on the surface of $NaYF_4$ particles and also prove the successful doping of Yb^{3+} and Er^{3+} ions.

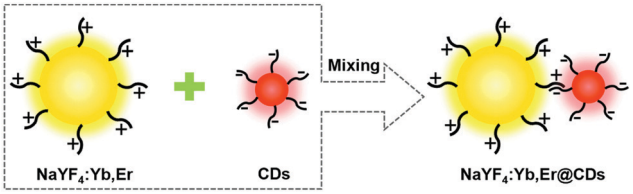

Scheme 1 Schematic illustration of the construction of $NaYF_4$:Yb,Er@CDs nanocomposites.

The crystal phase and surface functional groups were investigated by X-ray diffraction (XRD), and Fourier transform infrared (FT-IR) spectroscopy. As shown in Fig. 2a, the diffraction peaks in the XRD pattern of $NaYF_4$:Yb,Er are well matched with the cubic $NaYF_4$ (JCPDS No. 77-2042). The weak and broad peak appearing in the XRD pattern of the $NaYF_4$:Yb,Er@CDs nanocomposites can generally be attributed to the amorphous CDs.[36,37] The surface functional groups of CDs, $NaYF_4$:Yb,Er, and $NaYF_4$:Yb,Er@CDs are shown in the FT-IR spectra of Fig. 2b. For the CDs, the broad absorption band at 3050–3600 cm^{-1} is assigned to the stretching vibrations of –OH/N–H. The characteristic peaks at 1640, 1580, and 1200 cm^{-1} indicate the presence of C═O, C═C, and C═S, respectively. Importantly, the absorption peak at 1350 cm^{-1} is ascribed to the vibration of carboxylate radicals (COO) in carboxylate groups, which are negatively charged groups. For the $NaYF_4$:Yb,Er UCNPs, the absorption band at 2750–3000 cm^{-1} and the absorption peak at 1450 cm^{-1} are attributed to the stretching and bending vibrations of CH_2, respectively. The broad absorption band at 3150–3650 cm^{-1} and the absorption peak at 1630 cm^{-1} are assigned to the vibrations of amine groups including NH_2 and NH in PEI ligands, which belong to positively charged groups. It can be seen that the absorption processes of related groups at 3150–3650 and 1630 cm^{-1} in the $NaYF_4$:Yb,Er@CDs were significantly enhanced, suggesting the adsorption of CDs. Furthermore, the zeta potentials of $NaYF_4$:Yb,Er and CDs were determined to be +40.3 mV and −42.9 mV (Table S1, ESI†), respectively, which directly indicated that CDs were adsorbed on the surface of $NaYF_4$:Yb,Er particles. Because part of the charges were offset, the zeta potential of the $NaYF_4$:Yb,Er@CDs composites was +10.8 mV, which further confirmed the successful combination of CDs and $NaYF_4$:Yb,Er owing to strong electrostatic interactions.

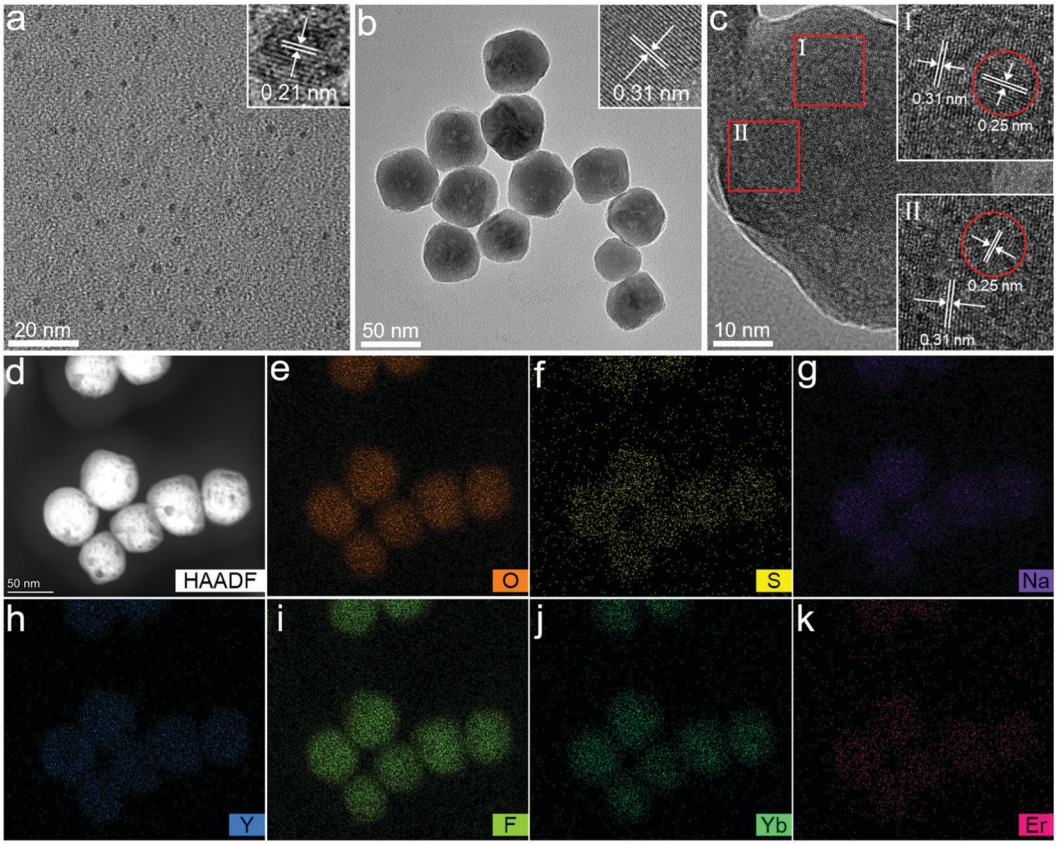

Fig. 1 (a) TEM and HRTEM images of CDs. (b) TEM and HRTEM images of $NaYF_4$:Yb,Er. (c) TEM images of $NaYF_4$:Yb,Er@CDs and the corresponding HRTEM images (the red circles show the CDs attached to the surface of $NaYF_4$:Yb,Er). (d–k) HAADF-STEM image and EDS elemental mapping of $NaYF_4$:Yb,Er@CDs (O and S for the CDs; Na, Y, F, Yb, and Er for $NaYF_4$:Yb,Er).

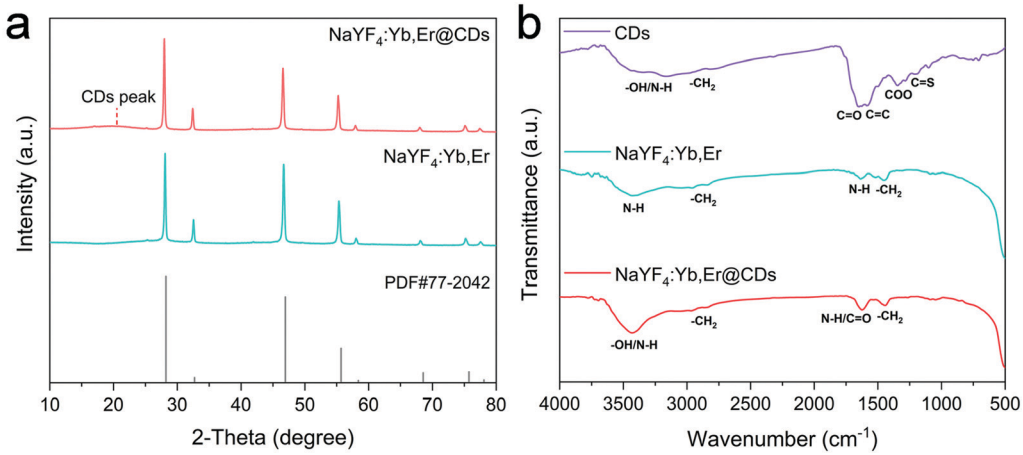

Fig. 2 (a) XRD patterns of $NaYF_4$:Yb,Er and $NaYF_4$:Yb,Er@CDs, and the standard diffraction data of cubic $NaYF_4$ (JCPDS No. 77-2042). (b) FT-IR spectra of CDs, $NaYF_4$:Yb,Er, and $NaYF_4$:Yb,Er@CDs.

The optical properties of CDs, $NaYF_4$:Yb,Er, and $NaYF_4$:Yb,Er@CDs were investigated by fluorescence spectroscopy and absorption spectroscopy. As shown in Fig. 3a, the as-prepared CDs in DMSO solution have dual-emission peaks, including blue and red peaks. Under low-wavelength UV excitation, the CDs mainly emit blue light. As the excitation wavelength increases, the red emission gradually dominates over the PL spectra. In particular, the CDs exhibit pure red emission at about 640 nm under the excitation of green light. Such CDs with polychromatic optical properties at different

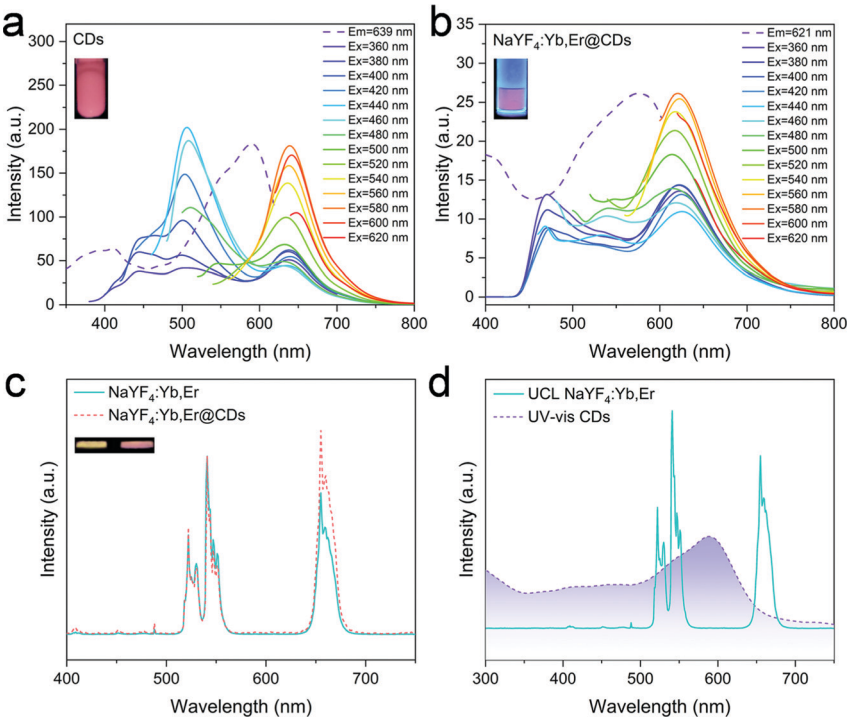

Fig. 3 (a) PL spectra of the CD solution; the inset shows the corresponding photograph of the CD solution under a 365 nm UV lamp. (b) PL spectra of $NaYF_4$:Yb,Er@CDs; the inset shows the corresponding photograph of $NaYF_4$:Yb,Er@CDs under a 365 nm UV lamp. (c) Normalized UCL spectra of $NaYF_4$:Yb,Er and $NaYF_4$:Yb,Er@CDs; the insets show the corresponding photographs of $NaYF_4$:Yb,Er (left) and $NaYF_4$:Yb,Er@CDs (right) under a 980 nm laser, respectively. (d) UV-vis absorption spectrum of CDs and UCL spectrum of $NaYF_4$:Yb,Er.

excitation wavelengths are favorable for application in luminescence anti-counterfeiting. The inset in Fig. 3a shows the fluorescence image of the CD solution under UV lamp irradiation. In the $NaYF_4$:Yb,Er@CDs nanocomposite powder, the CDs are uniformly adsorbed on the surface polymer ligand chains of $NaYF_4$:Yb,Er particles, which can overcome the aggregation-caused quenching effect of solid CDs and consequently maintain the same fluorescence emission as in the solution. Therefore, we can observe the emission of CDs from the PL spectra of the $NaYF_4$:Yb,Er@CDs nanocomposites in Fig. 3b. The inset shows the fluorescence image of the $NaYF_4$:Yb,Er@CDs nanocomposites under UV light irradiation, which is similar to that of the CD solution in the inset of Fig. 3a. As shown in Fig. 3c, the normalized UCL spectra of $NaYF_4$:Yb,Er and $NaYF_4$:Yb,Er@CDs nanocomposites have the same emission peaks at 522 nm, 541 nm, and 654 nm. The images of $NaYF_4$:Yb,Er and $NaYF_4$:Yb,Er@CDs nanocomposites under 980 nm laser irradiation are shown in the insets of Fig. 3c. A notable phenomenon is that the red emission of $NaYF_4$:Yb,Er@CDs nanocomposites is more stronger than that of pure $NaYF_4$:Yb,Er (Fig. 3c and Fig. S3, ESI†), implying the existence of energy transfer between $NaYF_4$:Yb,Er and CDs. Furthermore, there are spectral overlaps between the absorption spectrum of CDs and the UCL spectrum of $NaYF_4$:Yb,Er (Fig. 3d), which provides a possibility for energy transfer from the green emission of Er^{3+} ions to CDs. In addition, the red emission wavelengths of CDs and $NaYF_4$:Yb,Er are very close, which is beneficial for the red emission of CDs to be transmitted back to the red emissive energy level of Er^{3+}, thus enhancing the red emission of $NaYF_4$:Yb,Er. The luminescence decay curves and lifetime data are shown in Fig. S4 and Table S2 (ESI†). The almost unaltered UC green luminescence lifetimes (Fig. S4a, ESI†) of $NaYF_4$:Yb,Er and $NaYF_4$:Yb,Er@CDs suggest the radiation reabsorption of the green emission of Er^{3+} ions by CDs. The reduced red luminescence lifetime (Fig. S4b, ESI†) of $NaYF_4$:Yb,Er@CDs compared to the pure CDs under 541 nm excitation as well as the enhanced UC red emission (Fig. 3c) of $NaYF_4$:Yb,Er@CDs indicates the energy transfer from the excited state of CDs to the red emissive energy level of Er^{3+} ions through the resonance energy transfer process. Therefore, the energy transfer mechanism here is similar but not identical to our previous work.[38] In addition, when such composites with internal energy transfer features are applied for anti-counterfeiting, it is difficult to imitate by using certain substitutes or simply mixing different luminescent materials. Taken together, the above results demonstrate that the $NaYF_4$:Yb,Er@CDs nanocomposites possess dual-mode luminescence properties, which also further proves the successful combination of $NaYF_4$:Yb,Er and CDs through electrostatic interactions. The structural stability of the $NaYF_4$:Yb,Er@CDs nanocomposites was also investigated. On the one hand, stable composite structures were obtained when the CDs were adsorbed on the surface of $NaYF_4$:Yb,Er. After 42 hours, the CDs were still not detached from the $NaYF_4$:Yb,Er surface (Fig. S5a, ESI†). On the other hand, even if the as-prepared $NaYF_4$:Yb,Er@CDs composites were immersed in common

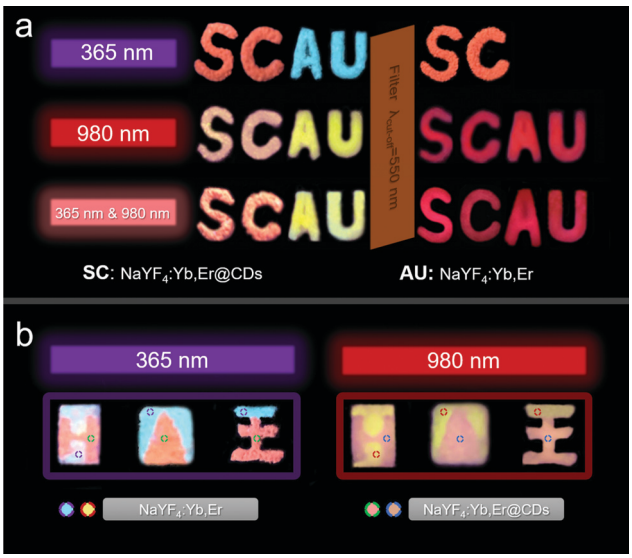

Fig. 4 (a) The photographs of "SCAU" patterns made with $NaYF_4$:Yb,Er@CDs and $NaYF_4$:Yb,Er under 365 nm, 980 nm, and 365 nm & 980 nm irradiation for dual-mode anti-counterfeiting. (b) The photographs of graphic security patterns made with $NaYF_4$:Yb,Er and $NaYF_4$:Yb,Er@CDs under 365 nm and 980 nm irradiation for dual-mode anti-counterfeiting.

organic solvents and water with shaking, the CDs were still not separated from the composites (Fig. S5b, ESI†). Thus, these results proved the good stability of the $NaYF_4$:Yb,Er@CDs composites.

Given the excellent dual-mode luminescence properties of $NaYF_4$:Yb,Er@CDs nanocomposites, they were used for dual-mode anti-counterfeiting applications. As shown in Fig. 4a, "SC" and "AU" patterns were made with $NaYF_4$:Yb,Er@CDs and $NaYF_4$:Yb,Er, respectively. These letter patterns display specific and multicolor images under the irradiation of 365 nm UV light, a 980 nm laser, and 365 nm UV light & a 980 nm laser, respectively, which reflects the multi-mode excitation characteristics. After using a 550 nm cut-off filter, the images with other colors can be read, which further improves the anti-counterfeiting level. In addition, some logos for graphic security made with $NaYF_4$:Yb,Er@CDs and $NaYF_4$:Yb,Er also show the role of dual-mode anti-counterfeiting in Fig. 4b. In short, it is meaningful for advanced anti-counterfeiting to gain particular information with different color characteristics by dual-mode excitation.

Conclusions

In summary, we have developed a simple and rapid construction strategy to prepare $NaYF_4$:Yb,Er@CDs nanocomposites which are suitable for dual-mode anti-counterfeiting technology. The surface potentials of PEI-modified $NaYF_4$:Yb,Er particles and carboxylate radical-functionalized CDs are exactly opposite. By simply mixing and oscillating $NaYF_4$:Yb,Er and CDs in solution, the efficient adsorption of CDs on the surface polymer ligand chains of $NaYF_4$:Yb,Er particles can be achieved in a very short time through electrostatic interactions, which also helps CDs to avoid the aggregation-caused quenching effect so that they can emit bright fluorescence in the solid state. Therefore, the resulting $NaYF_4$:Yb,Er@CDs nanocomposites have superior dual-mode luminescence properties, including the UCL of $NaYF_4$:Yb,Er and the DCL of CDs. As a proof of the prospective application, a preliminary demonstration of the dual-mode anti-counterfeiting scheme is carried out. Finally, more studies are expected to be performed such as the realization of tunable dual-mode luminescence by changing the kinds of rare earth ions and using different luminescent CDs.

Conflicts of interest

The authors declare no competing financial interest.

Acknowledgements

This work was supported by the National Natural Science Foundation of China (52172142 and 12174119), the Guangdong Basic and Applied Basic Research Foundation (2020A1515011210 and 2022A1515011958), the Science and Technology Planning Project of Guangdong Province (2021A0505060007), and the Science and Technology Planning Project of Guangzhou City (202102080288 and 202007020005).

References

1 X. Yu, H. Zhang and J. Yu, *Aggregate*, 2021, **2**, 20–34.
2 P. Kumar, S. Singh and B. K. Gupta, *Nanoscale*, 2016, **8**, 14297–14340.
3 B. Song, H. Wang, Y. Zhong, B. Chu, Y. Su and Y. He, *Nanoscale*, 2018, **10**, 1617–1621.
4 A. F. Smith and S. E. Skrabalak, *J. Mater. Chem. C*, 2017, **5**, 3207–3215.
5 W. Ren, G. Lin, C. Clarke, J. Zhou and D. Jin, *Adv. Mater.*, 2019, **32**, 1901430.
6 J. Yuan, P. R. Christensen and M. O. Wolf, *Chem. Sci.*, 2019, **10**, 10113–10121.
7 K. Du, M. Zhang, Y. Li, H. Li, K. Liu, C. Li, J. Feng and H. Zhang, *Adv. Opt. Mater.*, 2021, **9**, 2100814.
8 D. Gao, J. Gao, F. Gao, Q. Kuang, Y. Pan, Y. Chen and Z. Pan, *J. Mater. Chem. C*, 2021, **9**, 16634–16644.
9 D. Gao, D. Zhao, Y. Pan, R. Chai, Q. Pang a, X. Zhang and W. Chen, *Ceram. Int.*, 2021, **47**, 32000–32007.
10 J. C. Kays, A. M. Saeboe, R. Toufanian, D. E. Kurant and A. M. Dennis, *Nano Lett.*, 2020, **20**, 1980–1991.
11 F. P. García de Arquer, D. V. Talapin, V. I. Klimov, Y. Arakawa, M. Bayer and E. H. Sargent, *Science*, 2021, 373.
12 L. Xu, S. Yuan, H. Zeng and J. Song, *Mater. Today Nano*, 2019, **6**, 100036.
13 S. Sun, M. Lu, X. Gao, Z. Shi, X. Bai, W. W. Yu and Y. Zhang, *Adv. Sci.*, 2021, **8**, 2102689.
14 M. Fang, J. Yang and Z. Li, *Prog. Mater. Sci.*, 2022, **125**, 100914.
15 Q. Li and Z. Li, *Acc. Chem. Res.*, 2020, **53**, 962–973.
16 B. Wang and S. Lu, *Matter*, 2022, **5**, 110–149.

17 T. C. Wareing, P. Gentile and A. N. Phan, *ACS Nano*, 2021, **15**, 15471–15501.
18 Z. Tian, X. Zhang, D. Li, D. Zhou, P. Jing, D. Shen, S. Qu, R. Zboril and A. L. Rogach, *Adv. Opt. Mater.*, 2017, **5**, 1700416.
19 Y. Zheng, H. Wei, P. Liang, X. Xu, X. Zhang, H. Li, C. Zhang, C. Hu, X. Zhang, B. Lei, W.-Y. Wong, Y. Liu and J. Zhuang, *Angew. Chem., Int. Ed.*, 2021, **60**, 22253–22259.
20 J. Ge, Q. Jia, W. Liu, L. Guo, Q. Liu, M. Lan, H. Zhang, X. Meng and P. Wang, *Adv. Mater.*, 2015, **27**, 4169–4177.
21 L. Ai, Y. Yang, B. Wang, J. Chang, Z. Tang, B. Yang and S. Lu, *Sci. Bull.*, 2021, **66**, 839–856.
22 Y. Zhai, Y. Wang, D. Li, D. Zhou, P. Jing, D. Shen and S. Qu, *J. Colloid Interface Sci.*, 2018, **528**, 281–288.
23 A. Xu, G. Wang, Y. Li, H. Dong, S. Yang, P. He and G. Ding, *Small*, 2020, **16**, 2004621.
24 X. Zhu, J. Zhang, J. Liu and Y. Zhang, *Adv. Sci.*, 2019, **6**, 1901358.
25 X. Zheng, R. K. Kankala, C.-G. Liu, S.-B. Wang, A.-Z. Chen and Y. Zhang, *Coord. Chem. Rev.*, 2021, **438**, 213870.
26 L. Sun, R. Wei, J. Feng and H. Zhang, *Coord. Chem. Rev.*, 2018, **364**, 10–32.
27 A. Sedlmeier and H. H. Gorris, *Chem. Soc. Rev.*, 2015, **44**, 1526–1560.
28 M. Li, W. Yao, J. Liu, Q. Tian, L. Liu, J. Ding, Q. Xue, Q. Lu and W. Wu, *J. Mater. Chem. C*, 2017, **5**, 6512–6520.
29 A. Zhou, F. Song, W. Yao, Y. Han, F. Song, W. Wu, C. Ming, D. Ju and A. Khan, *J. Alloys Compd.*, 2019, **775**, 457–465.
30 X. Xu, W. Li, W. Zhou, G. Tan, Y. Zheng, C. Hu, B. Lei, X. Zhang, Y. Liu and J. Zhuang, *J. Mater. Chem. C*, 2018, **6**, 10360–10366.
31 H. Tan, G. Gong, S. Xie, Y. Song, C. Zhang, N. Li, D. Zhang, L. Xu, J. Xu and J. Zheng, *Langmuir*, 2019, **35**, 11503–11511.
32 D. Zhang, L. Wen, R. Huang, H. Wang, X. Hu and D. Xing, *Biomaterials*, 2018, **153**, 14–26.
33 X. Guo, C.-F. Wang, Z.-Y. Yu, L. Chen and S. Chen, *Chem. Commun.*, 2012, **48**, 2692.
34 H. Nie, M. Li, Q. Li, S. Liang, Y. Tan, L. Sheng, W. Shi and S. X.-A. Zhang, *Chem. Mater.*, 2014, **26**, 3104–3112.
35 J. Liu, D. Li, K. Zhang, M. Yang, H. Sun and B. Yang, *Small*, 2018, **14**, 1703919.
36 X. Miao, D. Qu, D. Yang, B. Nie, Y. Zhao, H. Fan and Z. Sun, *Adv. Mater.*, 2017, **30**, 1704740.
37 Y. Chen, M. Zheng, Y. Xiao, H. Dong, H. Zhang, J. Zhuang, H. Hu, B. Lei and Y. Liu, *Adv. Mater.*, 2016, **28**, 312–318.
38 X. Xu, X. Zhang, C. Hu, Y. Zheng, B. Lei, Y. Liu and J. Zhuang, *J. Mater. Chem. C*, 2019, **7**, 6231–6235.